Ultrafast modification of band structure of wide-band-gap solids by ultrashort pulses of laser-driven electron oscillations

Vitaly Gruzdev and Olga Sergaeva

Phys. Rev. B **98**, 115202 — Published 17 September 2018

DOI: 10.1103/PhysRevB.98.115202

Ultrafast modification of band structure of wide-band-gap solids by ultrashort pulses of laser-driven electron oscillations

Vitaly Gruzdev[1,*] and Olga Sergaeva[1,2,†]

[1] *Department of Mechanical and Aerospace Engineering, University of Missouri, Columbia, MO, 65211, USA*
[2] *ITMO University, St. Petersburg 197101, Russia*

(Dated: August 24, 2018)

The electric field of high-intensity ultrashort laser pulses substantially perturbs electron sub-system of a crystal and affects its band structure. Laser-driven oscillations of electrons and holes are frequently referred to as a major mechanism of the perturbation in dielectrics and semiconductors. New physical effects arise when the band structure is modified by an ultrashort pulse of the oscillations driven by a few-cycle laser pulse. Assuming the laser-pulse envelope varies slowly compared to the carrier frequency, we derive analytical relations for the laser-modified band structure by utilizing the Keldysh cycle-averaged non-perturbative approach under the approximation of constant effective mass. Formation of indirect-gap transient bands, suppression of the nonlinear absorption on the leading edge of a laser pulse, and cycle-averaged photo-current generation driven by the pulse envelope are predicted. Analytical scaling with six laser and material parameters is obtained. The reported results establish the limits of validity of the Keldysh photoionization model and advance understanding of the fundamental effects involved in high-intensity ultrafast laser-solid interactions.

PACS numbers: 71.20.-b; 78.47.J- ; 78.20.-e.

I. INTRODUCTION

Ultrafast laser interaction with electron sub-system of non-metal solids has been under intensive studies for several decades [1–45]. The strong interest to that field results from the fundamental fact: the laser-electron interaction and energy deposition into the electron sub-system substantially contribute to all high-intensity ultrafast laser interactions with wide-band-gap crystals, e.g., laser ablation [1–8], laser-induced damage [7–15], excitation of transient optical response [16–18], direct writing of nanostructures [19, 20], and ultrafast nonlinear propagation [21–24]. A recent development of petawatt (PW) laser systems launched another wave of research activity in this field [25]. The general approach to reach the PW domain of laser-pulse power is to reduce pulse width towards the femtosecond range [25]. Therefore, the electron sub-system of optical materials of the PW lasers interacts with the optical radiation of PW peak power concentrated within femtosecond-long pulse.

Exceptionally high peak irradiance characteristic of those interactions (that exceeds 10 TW/cm^2) is frequently acknowledged as one of the major contributors to the novel physical effects, e.g., generation of very high order harmonics (HHG) and ultrafast strong-field laser effects [26–45]. Corresponding peak value of laser-pulse electric field E_0 is close to or even higher than the characteristic electric field of a crystal lattice $E_{CR} = \Delta/(d \cdot q)$ estimated via band gap Δ, crystal-lattice constant d, and electron charge q [46]. Therefore, the laser pulses significantly distort the electron sub-system and its energy spectrum, i.e., band structure, and those distortions cannot be treated by a regular time-dependent perturbation theory [47], but require non-perturbative approaches.

Currently, there are two major groups of the non-perturbative approaches employed to simulate the ultrafast laser interaction with electrons of the solids. The first one brings together various numerical methods to solve time-dependent quantum-mechanical equations. The most sophisticated are the *ab initio* simulations by direct numerical solving the time-dependent Schrodinger equation [36–42, 48–53]. Those approaches deliver the most detailed information on sub-cycle electron dynamics driven by instant electric field of a laser pulse, e.g., instant 3D distribution of electron density. However, they are time-consuming, effectively treat the dynamics only over a limited time range (typically about 10-20 femtoseconds). Due to that reason, they meet substantial challenges in the proper implementation of electron-phonon collisions for realistic 3D crystal structures with multiple energy bands. To overcome those limitations, reduced or simplified numerical approaches are utilized, e.g., solving 1D or 2D Schrodinger equation for a truncated set of electron functions of few energy bands [36–42]; reduction of the Schrodinger equation to the semiconductor Bloch or matrix-element equations [29–35]; semi-analytical models [43, 44], and empirical pseudopotential methods [45]. Although the numerical modeling currently dominates in theoretical studies of the non-perturbative laser-electron interactions [29–44, 49–53], it faces substantial challenges in simulations of scaling with laser and material parameters. Also, those approaches are not employed to simulate the laser-induced band-structure modification in spite of that it is one of the most fundamental aspects of the ultrafast laser-solid interactions that substantially assists

* gruzdevvitaly@hotmail.com; Current affiliation: Department of Physics and Astronomy, The University of New Mexico, Albuquerque, NM, 87131, USA
† olgasergayeva@gmail.com

in understanding the physics of the interactions.

The other group of the non-perturbative approaches operates with cycle-averaged electron transition/excitation rates. Correspondingly, those approaches consider slow time variations driven by pulse envelope rather than the sub-cycle dynamics driven by instant electric field of a laser pulse. They employ the approximation of decoupled inter- and intra-band laser-driven excitations [1, 2, 4, 5, 7–12, 18–24]. In particular, the approaches of this group use the Keldysh formula [54] to evaluate the rate of the field-driven inter-band transitions that is not coupled to electron-particle collision and intra-band absorption rates of conduction-band electrons.

Although the models of this group are approximate, they have several advantages. They provide transparent interpretation of the experimental data and significantly assist in identifying specific contributions to the overall interactions. They deliver analytical scaling of the laser-induced effects with laser and material parameters due to the use of analytical formulae for the rates of the electron excitations [1, 2, 4, 5, 7–12, 18–24]. The analytical models are a highly supporting complement to the numerical simulations and are indispensable for qualitative analysis of the physics of ultrafast high-intensity laser interaction with quantum systems [55]. In particular, they are pivotal tools in studies of the non-trivial influence of band-structure on the photoionization rate [56–59]. Finally, the approximate analytical approaches take into account the laser-induced modification of the energy bands when evaluating the inter-band excitation rate. In the first approximation, the band modification is assumed to result from the ponderomotive energy of intra-band laser-driven electron oscillations [54, 59].

However, all the electron-transition rates employed by the analytical approaches are evaluated under the monochromatic approximation. It implies single-frequency cosine variations of electric field at constant amplitude that is in obvious contradiction with realistic time variations of electric field of a laser pulse. The usual way to overcome this issue is to replace the constant electric-field amplitude with the slowly varying amplitude of a pulse envelope [1, 2, 4, 5, 7–12, 14–24]. Although this approach raises significant concerns, e.g., when the monochromatic Keldysh formula is applied to laser pulses containing 2-25 cycles [22, 60–62], no analysis has been done so far to determine a range of laser parameters where such modification of the monochromatic approximation is valid.

Therefore, there are several significant gaps in the studies of the ultrafast high-intensity laser interactions with electrons of the solids for pulse durations from few cycles to few tens of cycles. In this pulse-width range, the validity of the simple analytical models is highly questionable due to the failure of the monochromatic approximation while the numerical approaches are not applied because of various reasons. Recently reported attempts to build analytical non-monochromatic models either assume low irradiance and the perturbative regime of the laser-electron interaction [60, 61] or are obtained by improper modifications of the Keldysh formula [22, 62]. However, exactly this range of pulse widths is of special significance for various applications, e.g., to support the development of the PW laser systems.

To fix this gap, we propose to use the Keldysh non-perturbative approach that serves as a basis for the Keldysh theory of the photoionization [54]. It assumes the major perturbation to the electron sub-system of a solid can be interpreted in terms of laser-driven oscillations of electrons and holes [59, 63]. The concept of the laser-driven electron oscillations in a crystal is so fundamental and powerful that the recent theoretical studies of the HHG and strong-field ultrafast solid-state effects frequently employ it [26–45]. According to it, energy gaps between electron states involved in the laser-induced inter-band transitions are modified by the amount of cycle-averaged ponderomotive energy of the oscillations [54, 59, 63, 64]. Therefore, modification of the energy gaps by the laser-driven oscillations can be interpreted in terms of formation of quasi-energy-bands obtained by adding the ponderomotive energy to the energy of the initial energy bands [59, 63].

With those motivations, here we report an analytical study of the high-intensity femtosecond laser-induced modifications of energy bands of a wide-band-gap crystal driven by the electron/hole oscillations. The bands of quasi-energy obtained under the approach described below are referred to as effective or transient bands. In Section II we describe the proposed model including a brief overview of the concept of the laser-driven electron/hole oscillations (II.1), qualitative analysis of the physics of the band-structure modifications (II.2), and the major approximations (II.3). Section III contains analytical relations for the direct-gap energy bands (III.1) and examples of modeling for Gaussian pulse envelope (III.2). Section IV discusses the obtained results including the contributions of different terms of the employed asymptotic series (IV.1); scaling with material and laser parameters (IV.2); other mechanisms of the band-structure modifications (IV.3); slowly-varying photocurrent (IV.4); the case of indirect-gap crystals (IV.5); and the impact of the reported results on the nonlinear absorption in the wide-band-gap crystals (IV.6). We finish with the major conclusions in Section V.

II. DESCRIPTION OF THE MODEL

II.1. Laser-driven electron/hole oscillations

Considering femtosecond pulses with the duration below 30 cycles, we neglect the atomic motion that takes significantly longer time in the crystals [65]. Accordingly, the only ultrafast distortion of the energy bands during an immediate laser-pulse action results from the laser-electron interaction in the crystal. Neglecting Coulomb-type interactions and applying the single-electron and dipole approximations [46, 64], one arrives at the following time-dependent Schrodinger equation in the length

gauge to describe the laser-electron interaction [64]:

$$i\hbar\frac{\partial\Psi(\vec{r},t)}{\partial t} = \hat{H}_0(\vec{r})\Psi(\vec{r},t) - q\vec{E}(t)\vec{r}, \quad (1)$$

where $\hat{H}_0(\vec{r})$ is the space-periodic non-perturbed Hamiltonian of the crystal. Approximate solutions to Eq. (1) are given by non-steady Bloch functions [54, 64, 66, 67]:

$$\psi(\vec{r},t) = u_{CB}(\vec{p}[t],\vec{r})exp\left(\frac{i}{\hbar}\vec{p}[t]\cdot\vec{r}\right) \times exp\left(-\frac{i}{\hbar}\int\limits_{-\infty}^{t}\varepsilon_{CB}(\vec{p}[\tau])d\tau\right), \quad (2)$$

where $u(\vec{p},\vec{r})$ is the amplitude of a steady Bloch function of the non-perturbed crystal Hamiltonian [46], and time-dependent electron momentum is expressed via the Bloch acceleration theorem [46, 64]:

$$\vec{p}(t) = \vec{p}_0 - q\int\limits_{-\infty}^{t}\vec{E}(\tau)d\tau, \quad (3)$$

where $p_0 = (p_{0x}, p_{0y}, p_{0z})$ is an initial value of 3D momentum. With the proper choice of time dependence of the electric field, the functions of Eqs. (2) and (3) have been successfully utilized for the non-perturbative evaluation of probabilities and rates of various effects, e.g., in the theory of the Franz-Keldysh effect [67], the Keldysh photoionization model [54], and studies of the strong-field ultrafast effects in the semiconductor crystals [39–44]. Below, we employ the approach based on the non-steady functions of Eq. (2) and propose an interpretation of the band-structure modifications using the oscillatory interpretation of the non-steady Bloch functions [26–30, 32, 38–44, 59, 63, 68–70].

In this connection, we note that the crystal-momentum oscillations of Eq. (3) driven by periodic time variations of the laser-pulse electric field are frequently referred to as Bloch oscillations [26–30, 32, 38, 39]. However, the true Bloch oscillations are produced by a *dc* electric field E_0 and are characterized by two specific features. First, momentum varies at constant rate [46, 63, 64, 66–70]:

$$\vec{p}(t) = \vec{p}_0 - qE_0t. \quad (4)$$

Second, the only physical mechanism of the periodicity of the electron motion is the multiple Bragg-type reflection of the electron at the edges of a Brillouin zone [59, 63, 64, 68–70]. Correspondingly, cycle duration of the Bloch oscillations T_{BO} is determined by the *dc* field and dimensions of the Brillouin zone. For example, if the field is parallel to a principle crystal axis, duration of the Bloch cycle reads as follows:

$$T_{BO} = \frac{2\pi\hbar}{qE_0d}, \quad (5)$$

where d is the crystal-lattice constant along that axis.

In case of the laser-driven electron oscillations, the periodicity of the electron motion results from the periodic time-domain variations of the driving *ac* electric field. Correspondingly, an electron is accelerated and decelerated at varying rate within a single cycle of the oscillations. Those oscillations are performed even if the amplitude of the laser-pulse electric field is so small that an oscillating electron does not reach the edges of the Brillouin zone and does not experience the Bragg-type reflections. At high laser intensity, the oscillating electrons can reach the edges of the zone and experience the Bragg-type reflections. If the duration of an optical cycle T_0 at the carrier frequency is significantly larger than the duration of the Bloch cycle T_{BO} at peak electric field of the laser pulse, the intra-band electron dynamics can be represented as the Bloch oscillations slowly modulated at the carrier frequency. For example, this is a good approximation for the THz frequency domain [30]. However, this is not the case for visible, near- and mid-infrared light, when an oscillating electron experiences just few Bragg-type reflections per optical cycle even at peak irradiance close to damage threshold [26–28]. To avoid confusions, here we consider the laser-driven oscillations of the electrons and holes driven at the carrier frequency in the visible, near-infrared or mid-infrared range of the optical spectrum and do not refer to them as Bloch oscillations.

II.2. Qualitative analysis

The concept of the laser-driven electron and hole oscillations provides a transparent interpretation of the band-structure modifications. To be specific, we consider an electron occupying an initial state at the bottom of the conduction band in the vicinity of the center of the Brillouin zone (state A in Fig. 1(a)). When affected by the electric field of linearly polarized monochromatic radiation, the electron performs intra-band single-frequency oscillations according to Eq. (3). Amplitude of electron departures from the initial state qE_0/ω_0 is of the same value for each half of each oscillation cycle (lower part of Fig. 1(a), blue dash-dotted cosine line), and the two ultimate states B and C reached by the electron at maximum departures are symmetrically located on the opposite sides of the Brillouin zone and the conduction band (Fig. 1(a)). The energy of the oscillating electron increases by the amount of average oscillation energy, i.e., ponderomotive energy U_{p0}:

$$U_{p0} = \frac{q^2E_0^2}{4m_{CB}\omega_0^2}, \quad (6)$$

where m_{CB} is effective conduction-band mass, and E_0 stays for the amplitude of the time-dependent laser-pulse electric field. Under the approximation of constant effective mass, the energy of all oscillating conduction-band electrons increases by the same amount given by Eq. (6). It results in a homogeneous distribution of the ponderomotive energy over the Brillouin zone. Correspondingly,

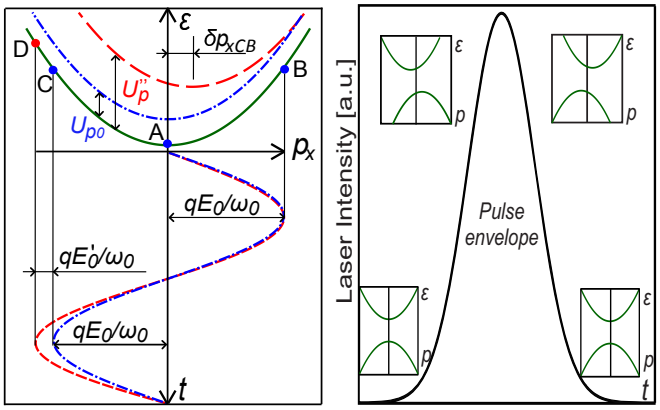

(a) (b)

FIG. 1. (a) Time variations of electron momentum due to the laser-driven oscillations (lower part) and associated modification of the conduction band (upper part) by the ponderomotive energy of the monochromatic (blue dash-dotted lines) and non-monochromatic (red dashed lines) oscillations. (b) Expected dynamics of the band p-shifts along a momentum direction parallel to electric field of a laser pulse: from the original direct-gap (left lower insert) via two oppositely shifted indirect-gap (upper inserts), and back to the original direct-gap bands (lower right insert).

the effective conduction band is produced from the original conduction band by homogeneous up-shifting in the energy space by the amount of the ponderomotive energy U_{p0}.

When the oscillations are driven by a linearly polarized ultrashort laser pulse, oscillation amplitude varies within each cycle, e.g., the second half of each oscillation cycle has a slightly larger amplitude ($qE_0/\omega_0 + qE_0'/\omega_0$) than the first half (at the leading edge of the pulse) (Fig. 1(a)). Due to this sub-cycle variation of the oscillation amplitude, the electron is dominantly promoted towards the part the Brillouin zone that hosts the lager departures of the oscillation cycles. For the sample electron of Fig. 1(a), that violation of the sub-cycle oscillation symmetry results in promoting the oscillating electron to the energy level D (Fig. 1(a)) that is higher than the level C reached by the monochromatic oscillation at the amplitude of the first half of the cycle. Furthermore, averaging of the oscillation energy over a single cycle delivers a non-homogeneous distribution of the ponderomotive energy U_p'' over the Brillouin zone, so that one part of the zone receives a larger amount of ponderomotive energy than the other (upper part of Fig. 1(a), red dashed curve). A simple geometrical consideration (Fig. 1(a)) suggests that the non-homogeneous distribution of ponderomotive energy leads to displacement of the bottom of the effective conduction band towards the part of the Brillouin zone that receives a smaller amount of ponderomotive energy. In case of a valence band, the laser-driven hole oscillations must result in similar effects except that all displacements are of opposite sign due to the positive charge of the holes. Therefore, the effective conduction and valence bands produced by the non-homogeneous distribution of ponderomotive energy are shifted in the opposite directions along the momentum axis parallel to the laser-pulse electric field. The considered band transformations are reversed at the tail edge of the pulse (Fig. 1(b)) and result in returning the modified bands back to their original positions in the energy-momentum space. However, the reverse dynamics of the modified bands must exhibit some delay since the electrons (and the holes) promoted to one side of the Brillouin zone cannot instantly return to the initial states.

This qualitative analysis suggests the formation of the indirect transient bands from the original direct bands due to the non-homogeneous distribution of ponderomotive energy of the laser-driven electron-hole oscillations. Correspondingly, the transient bands should be characterized by direct and indirect effective band gaps. Moreover, the considered dynamics of the shift of the energy bands suggests that the direct effective band gap of the transient bands must be larger than the effective band gap of the monochromatic approximation at the leading edge of the pulse. The situation is reversed at the rear edge of the pulse due to the delay of the reverse dynamics of the band modification. Moreover, because of the delay effects, the maximum direct effective band gap must be reached at a time instant that is shifted away from the laser-pulse peak.

II.3. Approximations and calculation procedure

To correctly introduce the modifications of the energy bands by an ultrashort pulse of the laser-driven electron oscillations, we assume that time variations of the electric field of a linearly polarized laser pulse are represented by a product of a slow envelope $f(t)$ and a fast oscillation at the carrier frequency ω_0:

$$\vec{E}(t) = \vec{E}_0 f\left(\frac{t}{\tau_p}\right)\cos(\omega_0 t + \phi_0), \tag{7}$$

where τ_p is a characteristic duration of the laser pulse, and ϕ_0 is a carrier-envelope phase (CEP) [27, 28, 39]. This assumption means that the pulse spectrum has an evident central frequency and is mathematically expressed via the following pulse parameter:

$$\alpha = \omega_0\tau_p = 2\pi\frac{\tau_p}{T_0} >> 1. \tag{8}$$

The assumption of Eq. (8) is met for pulses longer than two cycles and allows extracting the slow time variations of the band structure driven by the pulse envelope. The pulse parameter is utilized below to build asymptotic expansions of the band-structure modifications that incorporate the monochromatic approximation as zero-order terms obtained at $1/\alpha = 0$. Below in this paper, the electric field of Eq. (7) is assumed to be the electric field in the crystal evaluated with the contributions from laser-induced polarization, screening due to collective electron response, and other many-body effects.

Following the general concept of the Keldysh approach [54], we suppose that the laser-driven intra-band electron and hole oscillations are the dominating perturbation of the electron sub-system. In particular, we neglect the influence of electron-particle collisions. Measured electron dephasing time (e.g. Ref. [71]) supports the validity of this approximation. Also, neglecting the electron-particle collisions is a very usual approximation of a majority of recently published theoretical models of the ultrafast electron dynamics in crystals [26–42, 45].

Another assumption employed below considers a negligible influence of the inter-band electron transitions on the intra-band oscillations and band-structure modifications. The inter-band excitations are orders-of-magnitude weaker in the wide-band-gap crystals than in the typical semiconductors [43] because the rate of the inter-band excitation exponentially depends on band gap [54, 55]. Also, the density of laser-induced conduction-band electrons experimentally detected at the intensity close to the damage threshold is rather low ($10^{17}-10^{20}$ cm^{-3} in typical dielectrics [8, 16, 18, 23], i.e., it is below 1% of the total valence-electron density [46]). Finally, the usual theoretical approaches to calculate the band structure of crystals neglect any inter-band electron dynamics and consider it as a perturbation to the band structure [46, 64]. We follow this traditional approach below.

By combining Eq. (3) with Eq. (7), one obtains the following relation for the time-dependent electron momentum driven by the laser-pulse electric field:

$$\vec{p}(t) = \vec{p}_0 - \frac{q\vec{E}_0}{\omega_0} \int\limits_{-\infty}^{\omega_0 t} f\left(\frac{h}{\alpha}\right) \cos(h+\phi_0) dh, \qquad (9)$$

where normalized time $h = \omega_0 t$ is introduced. Momentum of a hole is represented by a similar expression with positive sign in front of the field-induced part. Asymptotically evaluating the integrals of Eq. (9), one arrives at the following expansion of time-dependent momentum with respect to small parameter $1/\alpha$:

$$\begin{aligned}\vec{p}(t) =& \vec{p}_0 - \frac{q\vec{E}_0}{\omega_0}\left[f\left(\frac{h}{\alpha}\right)\sin(h+\phi_0)) \right.\\ &+\frac{1}{\alpha} f'\left(\frac{h}{\alpha}\right)\cos(h+\phi_0) - \frac{1}{\alpha^2} f''\left(\frac{h}{\alpha}\right)\sin(h+\phi_0)\\ &\left.-\frac{1}{\alpha^3} f'''\left(\frac{h}{\alpha}\right)\cos(h+\phi_0)\right], \qquad (10)\end{aligned}$$

where $f'(x) = df(x)/dx$. Below we consider 3D momentum space, assume that the electric field is parallel to the axis Ox of the Brillouin zone, and consider two uncoupled energy bands – the lowest conduction and the highest valence – under the approximation of constant effective mass:

$$\varepsilon_{CB}(\vec{p}) = \Delta\left[1 + \frac{p_x^2+p_y^2+p_z^2}{2m_{CB}\Delta}\right], \qquad (11a)$$

$$\varepsilon_{VB}(\vec{p}) = -\Delta\left[\frac{p_x^2+p_y^2+p_z^2}{2m_{VB}\Delta}\right], \qquad (11b)$$

where Δ is the original (i.e., pre-laser) band gap, m_{CB} and m_{VB} are effective masses of the conduction (CB) and valence (VB) band correspondingly. The bands are direct-gap, i.e., the minimum energy gap between them is in the center of the first Brillouin zone. The energy-momentum relations of Eqs. (11) are rough for a proper description of the Bragg-type reflections of the oscillating electrons and holes at the edges of the Brillouin zone at high intensity [59, 63]. However, it does not affect the major mechanism of the periodicity of the laser-driven electron/hole oscillations outlined in Section II.2. Therefore, the approximation of Eqs. (11) is sufficient to uncover the major features of the band-structure modification under consideration, and the Bragg-type reflections of the electrons/holes can be treated as a distortion to be considered for later improvements of our approach.

Following the approximation of the Keldysh model [54] rigorously justified in Ref. [64], we first evaluate the laser-distorted energy bands by substituting the time-dependent momentum of Eq. (9) into the energy-momentum relations of Eq. (11). For example, the effective conduction band reads as follows:

$$\begin{aligned}\tilde{\varepsilon}_{CB}(\vec{p}_0,t) &= \varepsilon\left(\vec{p}_0 - q\int\limits_{-\infty}^{t}\vec{E}(\tau)d\tau\right)\\ &= \Delta\left(1 + \frac{p_0^2}{2m_{CB}\Delta} - \frac{x_{CB}}{\gamma_{CB}}\int\limits_{-\infty}^{\omega_0 t} f\left(\frac{h}{\alpha}\right)\cos(h+\phi_0)dh\right.\\ &\left.+\frac{1}{2\gamma_{CB}^2}\left[\int\limits_{-\infty}^{\omega_0 t} f\left(\frac{h}{\alpha}\right)\cos(h+\phi_0)dh\right]^2\right), \qquad (12)\end{aligned}$$

where $x_{CB} = p_{0x}/\sqrt{m_{CB}\Delta}$ is normalized momentum component parallel to the laser-pulse electric field. Following the definition of Keldysh [54], we introduce the following band-specific and general Keldysh parameters:

$$\gamma_i = \frac{\omega_0\sqrt{m_i\Delta}}{qE_0};\ i = CB, VB, 0;\ \frac{1}{m_0} = \frac{1}{m_{CB}} + \frac{1}{m_{VB}}. \qquad (13)$$

The calculations are done as follows. Eq. (12) and a similar relation for the valence band are averaged over a single cycle T_0 of the carrier frequency to obtain equations for the transient slowly-varying energy bands that include the ponderomotive energy of the laser-driven electron/hole oscillations. Those cycle-averaged relations are asymptotically expanded into series with respect to the small parameter $1/\alpha$. The zero-order terms of the series correspond to the monochromatic approximation, and our studies are focused on the effects described by the higher-order terms.

III. MAJOR RESULTS

The advantage of the proposed approach is that it delivers analytical relations for arbitrary pulse envelope. Numerical evaluation of the transient bands is done for a particular case of Gaussian laser-pulse envelope.

III.1. Analytical relations for direct-gap bands: general case

The asymptotic expansions for the effective conduction band:

$$\varepsilon_{CB}^{eff}(\vec{p}_0,s)=\Delta\left[1+\frac{p_0^2}{2m_{CB}\Delta}+\frac{f(s)^2}{4\gamma_{CB}^2}\right. \tag{14}$$
$$+\frac{f'(s)}{\alpha}\left\{\frac{f(s)}{4\gamma_{CB}^2}[2\pi-\sin(2\phi_0)]+\frac{x_{CB}}{\gamma_{CB}}\cos(\phi_0)\right\}$$
$$+\frac{1}{\alpha^2}\left\{\frac{f'(s)^2}{4\gamma_{CB}^2}\Psi+\frac{f(s)f''(s)}{4\gamma_{CB}^2}(\Psi-3)-\frac{x_{CB}f''(s)}{\gamma_{CB}}\Psi_{x1}\right\}$$
$$\left.+\frac{1}{\alpha^3}\left\{\frac{f(s)f'''(s)}{4\gamma_{CB}^2}\Psi_1+\frac{f'(s)f''(s)}{4\gamma_{CB}^2}\Psi_2-\frac{x_{CB}f'''(s)}{\gamma_{CB}}\Psi_{x2}\right\}\right]$$

and effective valence band:

$$\varepsilon_{VB}^{eff}(\vec{p}_0,s)=-\Delta\left[\frac{p_0^2}{2m_{VB}\Delta}+\frac{f(s)^2}{4\gamma_{VB}^2}\right. \tag{15}$$
$$+\frac{f'(s)}{\alpha}\left\{\frac{f(s)}{4\gamma_{VB}^2}[2\pi-\sin(2\phi_0)]-\frac{x_{VB}}{\gamma_{VB}}\cos(\phi_0)\right\}$$
$$+\frac{1}{\alpha^2}\left\{\frac{f'(s)^2}{4\gamma_{VB}^2}\Psi+\frac{f(s)f''(s)}{4\gamma_{CB}^2}(\Psi-3)+\frac{x_{VB}f''(s)}{\gamma_{VB}}\Psi_{x1}\right\}$$
$$\left.+\frac{1}{\alpha^3}\left\{\frac{f(s)f'''(s)}{4\gamma_{VB}^2}\Psi_1+\frac{f'(s)f''(s)}{4\gamma_{VB}^2}\Psi_2+\frac{x_{VB}f'''(s)}{\gamma_{VB}}\Psi_{x2}\right\}\right]$$

include the terms of the asymptotic series of all orders from zero to $1/\alpha^3$. Here and below $s=t/\tau_p$ is the normalized time, and the following functions are introduced for the sake of compactness:

$$\Psi=\frac{4\pi^2}{3}+\frac{5}{2}-3\cos(\phi_0)^2-\pi\sin(2\phi_0), \tag{16a}$$
$$\Psi_1=\frac{2\pi^3}{3}-\frac{\pi}{2}-3\pi\cos(\phi_0)^2-\left(\frac{2\pi^2}{3}-\frac{7}{4}\right)\sin(2\phi_0), \tag{16b}$$
$$\Psi_2=2\pi^3+\frac{9\pi}{2}-9\pi\cos(\phi_0)^2-\left(2\pi^2-\frac{17}{4}\right)\sin(2\phi_0), \tag{16c}$$
$$\Psi_{x1}=2\sin(\phi_0)-\pi\cos(\phi_0), \tag{16d}$$
$$\Psi_{x2}=2\pi\sin(\phi_0)-\left(\frac{2\pi^2}{3}-3\right)\cos(\phi_0). \tag{16e}$$

The zero-order terms of the square bracket of Eqs. (14) and (15) correspond to the initial parabolic energy bands homogeneously shifted by the amount of ponderomotive energy evaluated under the monochromatic approximation. The $1/\alpha$, $1/\alpha^2$, and $1/\alpha^3$ terms of the square bracket describe the effects produced beyond the monochromatic approximation.

Time-dependent position of the bottom state of the effective conduction band:

$$p_{xCB}(s)=\sqrt{m_{CB}\Delta}\left[-\frac{f'(s)}{\alpha\gamma_{CB}}\cos(\phi_0)+\frac{f''(s)}{\alpha^2\gamma_{CB}}\Psi_{x1}\right.$$
$$\left.+\frac{f'''(s)}{\alpha^3\gamma_{CB}}\Psi_{x2}\right],$$
$$p_{yCB}(s)=p_{zCB}(s)=0, \tag{17}$$

confirms that the effective band is shifted along the momentum direction parallel to the laser-pulse electric field. Combining Eq. (17) with a similar equation for the position of the top state of the effective valence band:

$$p_{xVB}(s)=\sqrt{m_{VB}\Delta}\left[\frac{f'(s)}{\alpha\gamma_{VB}}\cos(\phi_0)-\frac{f''(s)}{\alpha^2\gamma_{VB}}\Psi_{x1}\right.$$
$$\left.-\frac{f'''(s)}{\alpha^3\gamma_{VB}}\Psi_{x2}\right],$$
$$p_{yVB}(s)=p_{zVB}(s)=0, \tag{18}$$

one arrives at a relation for the mutual p-shift of the transient bands:

$$\delta p_x(s)=p_{xCB}(s)-p_{xVB}(s) \tag{19}$$
$$=\frac{2\sqrt{m_0\Delta}}{\gamma_0}\left[-\frac{f'(s)}{\alpha}\cos(\phi_0)+\frac{f''(s)}{\alpha^2}\Psi_{x1}+\frac{f'''(s)}{\alpha^3}\Psi_{x2}\right],$$

where the band-specific adiabatic parameters are replaced with the usual Keldysh parameter of Eq. (13).

To fully characterize the indirect-gap structure of the transient bands, direct and indirect effective band gaps should be evaluated. The effective indirect band gap is determined as the minimum energy gap between the bottom of the effective conduction band of Eq. (14) and the top state of the effective valence band of Eq. (15):

$$\Delta_{ind}^{eff}(s)=\Delta\left[1+\frac{f(s)^2}{4\gamma_0^2}+\frac{f'(s)f(s)}{4\alpha\gamma_0^2}[2\pi-\sin(2\phi_0)]\right.$$
$$+\frac{f'(s)^2}{4\alpha^2\gamma_0^2}(\Psi-2\cos(\phi_0)^2)+\frac{f(s)f''(s)}{4\alpha^2\gamma_0^2}(\Psi-3) \tag{20}$$
$$\left.+\frac{f(s)f'''(s)}{4\alpha^3\gamma_0^2}\Psi_1+\frac{f'(s)f''(s)}{4\alpha^3\gamma_0^2}\big(\Psi_2-4\pi\cos(\phi_0)^2+4\sin(2\phi_0)\big)\right].$$

The effective direct band gap is evaluated as minimum of the function $\varepsilon(\vec{p}_0,s)=\varepsilon_{CB}^{eff}(\vec{p}_0,s)-\varepsilon_{VB}^{eff}(\vec{p}_0,s)$ and

reads as follows:

$$\Delta_{dir}^{eff}(s) = \Delta\Bigg\{1 + \frac{f(s)^2}{4\gamma_0^2} + \frac{f'(s)f(s)}{4\alpha\gamma_0^2}[2\pi - \sin(2\phi_0)]$$
$$+\frac{f'(s)^2}{4\alpha^2\gamma_0^2}\left[\Psi - 2\cos(\phi_0)^2\left[\frac{m_0}{m_{CB}} - \frac{m_0}{m_{VB}}\right]^2\right] \quad (21)$$
$$+\frac{f(s)f''(s)}{4\alpha^2\gamma_0^2}(\Psi - 3) + \frac{f(s)f'''(s)}{4\alpha^3\gamma_0^2}\Psi_1 + \frac{f'(s)f''(s)}{4\alpha^3\gamma_0^2}$$
$$\times\left[\Psi_2 + 4\left[\frac{m_0}{m_{CB}} - \frac{m_0}{m_{VB}}\right]^2[\sin(2\phi_0) - \pi\cos(\phi_0)^2]\right]\Bigg\}.$$

Position of the direct bag gap in the momentum space reads as follows:

$$p_{xDG}(s) = \sqrt{m_0\Delta}\left[\frac{m_0}{m_{CB}} - \frac{m_0}{m_{VB}}\right]$$
$$\times\left[-\frac{f'(s)}{\alpha\gamma_0}\cos(\phi_0) + \frac{f''(s)}{\alpha^2\gamma_0}\Psi_{x1} + \frac{f'''(s)}{\alpha^3\gamma_0}\Psi_{x2}\right],$$
$$p_{yDG}(s) = p_{zDG}(s) = 0. \quad (22)$$

The zero-order terms of the asymptotic expansions of Eqs. (20) and (21) exactly correspond to the effective band gap of the original Keldysh model produced under the monochromatic approximation [54]:

$$\Delta_{mh}^{eff}(s) = \Delta\left[1 + \frac{f(s)^2}{4\gamma_0^2}\right]. \quad (23)$$

It predicts conservation of the initial direct-gap structure of the effective bands. The contributions of the higher-order terms of Eqs. (20) and (21) result in formation of the indirect-gap transient bands.

III.2. Numerical evaluations: Gaussian pulse, direct-gap bands

The general relations of the previous section deliver more detailed information about the dynamics of the effective band structure if a pulse envelope is specified. Here we provide an illustrative analysis and simulation of the band-structure modifications for the Gaussian envelope:

$$f(s) = \exp(-s^2) = \exp\left(-\frac{t^2}{\tau_p^2}\right). \quad (24)$$

We note that the half-width τ_p of the electric-field pulse envelope of Eq. (24) is almost 1.7 times smaller than half-width $\tau_{HW} = \sqrt{\ln 2/2}\,\tau_p$ of a laser pulse at the level of 1/2 of peak intensity. For the numerical simulations, the laser-pulse peak intensity is below the threshold of laser-induced damage by few-cycle pulses [9–16, 26, 36, 37]. Material parameters are chosen to compare band-structure modifications in two crystals of different groups: a typical dielectric (NaCl) and a typical wide-band-gap semiconductor (AlN) (see Table I).

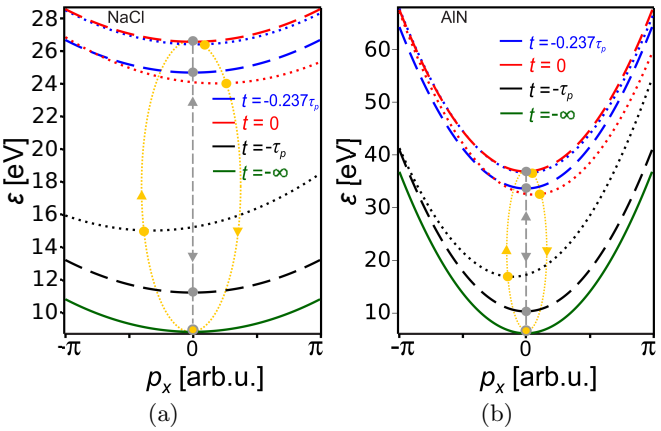

FIG. 2. Original conduction band (green solid) and transient bands (black, blue, red) evaluated for a Gaussian pulse envelope (Eq. (24); peak intensity 30 TW/cm^2; carrier wavelength 2400 nm; pulse half-width at the level $1/e$ of maximum intensity is 15 fs; zero CEP) at several instants of time for (a) NaCl and (b) AlN crystals under the monochromatic (Eq. (23); dashed lines) and pulse-driven (Eq. (14); dotted lines) approximations. Orange dots on the closed dotted curve and gray dots on the vertical gray dashed line depict positions of the bottom of the transient conduction bands on their laser-driven trajectories for the pulse-driven and monochromatic models correspondingly.

Figure 2 confirms the qualitative discussion of Section II.2 regarding dynamics of the effective-band variations by an ultrashort pulse of the laser-driven electron oscillations (see also Ref. [74]). In particular, the bottom point of the effective conduction band shifts along the momentum direction parallel to the laser-pulse electric field and makes an elliptic trajectory in energy-momentum space (Fig. 2) instead of a linear trajectory with zero p-shift characteristic of the monochromatic approximation of the original Keldysh model.

The simulations show very pronounced mutual p-shift of the transient conduction and valence bands in the momentum space even at moderate peak intensity and pulse width (Fig. 2 and 3). A significant influence of the envelope phase on the shift is highly remarkable (Fig. 3). In the time domain, the major features of that influence are: (a) the suppression of the band p-shifts with the formation of three maxima/minima separated by two zero-shift points if CEP is $\phi_0 = \pi/2 \pm N\pi$ (N=0;1;2;...) (Fig. 3); and (b) formation of one maximum and one minimum of the p-shift separated by a single zero-shift point if CEP

TABLE I. Material parameters utilized in simulations.

Parameter name	NaCl [72]	AlN [73]
Direct band gap, eV	8.9	6.2
Conduction-band effective mass, units of free-electron mass	0.6	0.25
Valence-band effective mass, units of free-electron mass	4.56	0.285

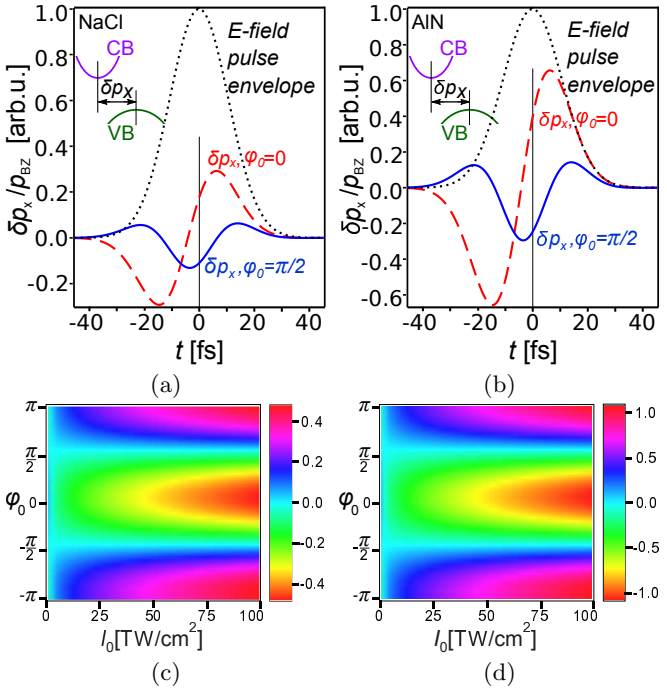

FIG. 3. (a, b): Normalized envelope of E-field pulse (black dotted) and time variations of the total mutual p-shift of the energy bands δp_x (Eq. (19)) normalized to the half-width of the first Brillouin zone p_{BZ} for (a) NaCl, and (b) AlN. Evaluation for the Gaussian envelope of Eq. (24) is done for two values of CEP: 0° (red dashed) and 90° (blue solid). The vertical solid lines mark the position of the pulse peak on the time axis for eye convenience. (c, d): Band shift δp_x normalized to p_{BZ} *vs* intensity I_0 and CEP ϕ_0 taken at fixed time instant $t = -\tau_p/\sqrt{2}$ for (c) NaCl; and (d) AlN. Parameters of the laser pulse are the same for all the panels: peak intensity is 30 TW/cm^2; carrier wavelength is 2400 nm; pulse half width at the level $1/e$ of maximum intensity is 15 fs.

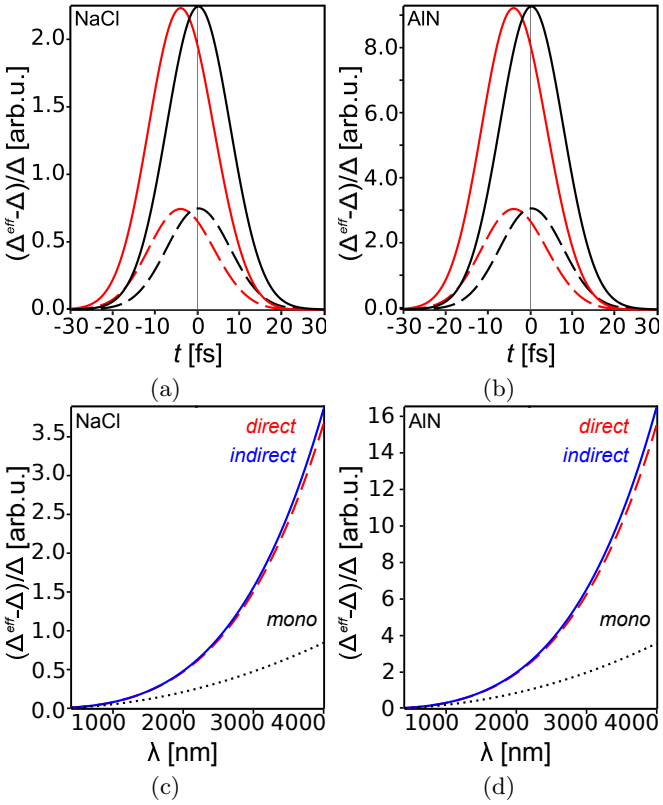

FIG. 4. (a, b) Normalized difference between the effective direct band gap and the original band gap for the monochromatic model of Eq. (23) (black curves) and the pulse-driven model of Eq. (21) (red curves) plotted *vs* time at peak laser intensity 10 TW/cm^2 (dashed curves) and 30 TW/cm^2 (solid curves) for (a) NaCl; and (b) AlN. Laser carrier wavelength is 2400 nm. The vertical solid lines mark the position of the pulse peak on the time axis for eye convenience. (c, d) Normalized difference between the laser-induced effective and original band gaps *vs* carrier wavelength for pulse-driven direct (Eq. (21); red solid); pulse-driven indirect (Eq. (20); blue dotted); and monochromatic (Eq. (23); black dashed) effective band gaps plotted at peak laser intensity 30 TW/cm^2 in (c) NaCl; and (d) AlN. The effective band-gap values are taken at time instant $t = -15$ fs. Other laser-pulse parameters are the same for all the panels: zero CEP; pulse half-width at the level $1/e$ of maximum intensity is 15 fs.

$\phi_0 \neq \pi/2 \pm N\pi$ (N=0;1;2;...) (Fig. 3). Also, Eq. (19) suggests that the absolute value of the mutual p-shift of the energy bands is of the order of $1/(\alpha^2\gamma_0)$ at the peak of a laser pulse (i.e., at t=0) at any value of the CEP.

Finally, we note that the pulse-driven model predicts maximum of both direct and indirect effective band gaps at the leading edge of the pulse (Fig. 4). Correspondingly, the effective band gaps exceed the value delivered by the monochromatic approximation of Eq. (23) at the leading edge of the laser pulse (Fig. 4). However, the pulse-induced effective band gaps are smaller than that of the monochromatic model at the tail part of the pulse (Fig. 4). The difference can be as large as few electron-volts depending on laser and material parameters. Also, a strong dependence of those non-monochromatic effects on laser wavelength is highly remarkable. In particular, the deviation of the pulse-driven model from the monochromatic approximation rapidly grows with increase of laser wavelength (Fig. 4 (c), (d)); also see Ref. [75] with animation of time variations of wavelength dependence of maximum effective direct and indirect band gaps).

The advantage of the reported above analytical model is the feasibility of a detailed characterization of the band-structure modification and dynamics (e.g., see Figs. 3 and 4) by rigorous analytical relations. For example, the maximum and minimum values of the mutual band p-shift at the CEP values $\phi_0 \neq \pi/2 \pm N\pi$, $N = 0, 1, 2, \ldots$ (Fig. 3), are analytically evaluated from Eq. (19):

$$\delta p_M(s_M) = \frac{2\sqrt{m_0\Delta}}{\alpha\gamma_0}\exp(-s_M^2) \tag{25}$$
$$\times\left\{\begin{array}{l}\pm\sqrt{2}\cos(\phi_0) + \dfrac{2}{\alpha}\Psi_{x1} \\ \mp\dfrac{2\sqrt{2}}{\alpha^2}\left[(4\pi - 6\tan(\phi_0))\sin(\phi_0) - \left(3 + \dfrac{11\pi^2}{6}\right)\cos(\phi_0)\right]\end{array}\right\},$$

and the time instants of the maximum and the minimum are also delivered by Eq. (19):

$$t_M = \tau_p \left[\pm \frac{1}{\sqrt{2}} + \frac{2\tan(\phi_0) - \pi}{\alpha} \mp \frac{\sqrt{2}}{\alpha^2} \left[3 + 2\tan(\phi_0)^2 - \frac{7\pi^2}{6} \right] \right], \tag{26}$$

where $s_M = t_M/\tau_p$. The three maxima and minima of the mutual bands p-shift at CEP $\phi_0 = \pi/2$ are analytically evaluated as follows:

$$\delta p_M(s_M, \phi_0 = \pi/2) = \\ = \left\{ \begin{array}{l} \frac{16\sqrt{m_0\Delta}}{\alpha^2\gamma_0} \left(1 + \frac{\sqrt{6}\pi}{\alpha} \right) \exp\left(- \left[\sqrt{\frac{3}{2}} + \frac{\pi}{\alpha} \right]^2 \right); \\ -\frac{8\sqrt{m_0\Delta}}{\alpha^2\gamma_0} \exp\left(-\frac{\pi^2}{\alpha^2} \right); \\ \frac{16\sqrt{m_0\Delta}}{\alpha^2\gamma_0} \left(1 - \frac{\sqrt{6}\pi}{\alpha} \right) \exp\left(- \left[\sqrt{\frac{3}{2}} - \frac{\pi}{\alpha} \right]^2 \right); \end{array} \right\}, \tag{27}$$

as well as the time instants when they appear:

$$t_M(\phi_0 = \pi/2) = \tau_p \left[-\sqrt{\frac{3}{2}} - \frac{\pi}{\alpha};\ -\frac{\pi}{\alpha};\ \sqrt{\frac{3}{2}} - \frac{\pi}{\alpha} \right]. \tag{28}$$

Analytical relations for other specific features of the band-structure modifications, e.g., time instants of the zero p-shift, have been reported before [76, 77].

The mutual band p-shift is not the only parameter significantly affected by CEP. Carrier-envelope phase substantially influences the time variations of effective indirect and direct band gaps as it is clear from the following relations:

(A) the time instants when the maximum effective indirect band gap is reached:

$$s_{MI} = \frac{\sin(2\phi_0) - 2\pi}{2\alpha} \\ + \frac{\sin(2\phi_0)}{\alpha^3} \left(11\sin(\phi_0)^2 + 2\cos(\phi_0)^4 + 2[2 - \cos(\phi_0)^2] \right), \tag{29}$$

(B) the maximum value of the *effective indirect band gap*:

$$\Delta^{eff}_{indMAX} = \\ = \Delta \left(1 + \frac{\exp(-2s_{MI}^2)}{4\gamma_0^2} \left[1 + \frac{(2\pi - \sin(2\phi_0))^2}{\alpha^2} - \frac{2\Psi - 6}{\alpha^2} \right] \right), \tag{30}$$

(C) the time instant of the maximum effective direct band gap:

$$s_{MD} = \frac{\sin(2\phi_0) - 2\pi}{2\alpha} \\ + \frac{\sin(2\phi_0)}{\alpha^3} \left(11\sin(\phi_0)^2 + 2\cos(\phi_0)^4 \right. \\ \left. + 2 \left[\frac{m_0}{m_{CB}} - \frac{m_0}{m_{VB}} \right]^2 [2 - \cos(\phi_0)^2] \right), \tag{31}$$

(D) and the maximum *effective direct band gap*:

$$\Delta^{eff}_{dirMAX} = \\ = \Delta \left(1 + \frac{\exp(-2s_{MD}^2)}{4\gamma_0^2} \left[1 + \frac{(2\pi - \sin(2\phi_0))^2}{\alpha^2} - \frac{2\Psi - 6}{\alpha^2} \right] \right). \tag{32}$$

IV. DISCUSSION

IV.1. Analysis of asymptotic contributions

The specific scaling of the band modification with parameters α, γ_{CB}, γ_{VB}, and γ_0 directly results from the inhomogeneous sub-cycle distribution of the oscillation amplitude explained in Section II.2. In this connection, we notice that the electric-field amplitude of the second half of any radiation cycle at arbitrary time instant t_2 can be expressed via the amplitude of the first half of the cycle at time instant $t_1 = t_2 - T_0/2$ by the following asymptotic series (for simplicity, zero CEP is assumed):

$$E_0 f\left(\frac{t_2}{\tau_p}\right) = E_0 f\left(\frac{t_1}{\tau_p}\right) + E_0 f'\left(\frac{t_1}{\tau_p}\right) \frac{T_0}{2\tau_p} \\ + \frac{E_0}{2} f''\left(\frac{t_1}{\tau_p}\right) \left(\frac{T_0}{2\tau_p}\right)^2 + \frac{E_0}{6} f'''\left(\frac{t_1}{\tau_p}\right) \left(\frac{T_0}{2\tau_p}\right)^3 \\ = E_0 f\left(\frac{t_1}{\tau_p}\right) + E_0 \frac{\pi}{\alpha} f'\left(\frac{t_1}{\tau_p}\right) + E_0 \frac{\pi^2}{2\alpha^2} f''\left(\frac{t_1}{\tau_p}\right) + E_0 \frac{\pi^3}{6\alpha^3} f'''\left(\frac{t_1}{\tau_p}\right), \tag{33}$$

obtained from Eq. (7) and (8). The amplitude $p_A(t_2)$ of the second half of the cycle of the conduction-electron oscillations driven by the electric field of Eq. (33) reads as follows:

$$p_A^{CB}(t_2) = \frac{qE_0}{\omega_0} f\left(\frac{t_2}{\tau_p}\right) = p_A^{CB}(t_1) + \frac{\pi\sqrt{m_{CB}\Delta}}{\alpha\gamma_{CB}} f'\left(\frac{t_1}{\tau_p}\right) \\ + \frac{\pi^2\sqrt{m_{CB}\Delta}}{2\alpha^2\gamma_{CB}} f''\left(\frac{t_1}{\tau_p}\right) + \frac{\pi^3\sqrt{m_{CB}\Delta}}{6\alpha^3\gamma_{CB}} f'''\left(\frac{t_1}{\tau_p}\right). \tag{34}$$

In Eq. (34), the second right-hand term delivers the amount of the violation of the homogeneous amplitude distribution within the cycle. The third term is associated with the rate of that effect and should be attributed to the delay effects discussed in Section II.2. For a valence-band hole, a relation similar to Eq. (34) can be obtained.

Eq. (34) shows that the difference $p_A(t_2) - p_A(t_1)$ contains the combinations of the parameters α and γ_{CB} with proper time derivations of the pulse envelope that are absolutely similar to those of Eq. (17) under the zero-CEP assumption. The same is true for the amplitude of the hole oscillations and Eq. (18).

Ponderomotive energy $U_{p0}(t_2)$ of the second half of the

oscillation cycle is expressed as follows by Eq. (33):

$$U_{p0}(t_2) = \frac{q^2 E_0^2}{4 m_{CB} \omega_0^2} f\left(\frac{t_1}{\tau_p}\right)^2 \tag{35}$$
$$= \frac{\Delta}{4\gamma_{CB}^2} \left[\begin{array}{l} f\left(\frac{t_1}{\tau_p}\right)^2 + \frac{2\pi}{\alpha} f\left(\frac{t_1}{\tau_p}\right) f'\left(\frac{t_1}{\tau_p}\right) \\ + \frac{\pi^2}{\alpha^2} f\left(\frac{t_1}{\tau_p}\right) f''\left(\frac{t_1}{\tau_p}\right) + \frac{\pi^2}{\alpha^2} f\left(\frac{t_1}{\tau_p}\right)^2 \\ + \frac{\pi^3}{3\alpha^3} f\left(\frac{t_1}{\tau_p}\right) f'''\left(\frac{t_1}{\tau_p}\right) + \frac{\pi^3}{\alpha^3} f\left(\frac{t_1}{\tau_p}\right) f''\left(\frac{t_1}{\tau_p}\right) \end{array} \right].$$

A similar relation can be obtained for the ponderomotive energy of the oscillating valence-band holes. The similarity between Eq. (35) and the field-dependent terms of Eq. (14) at zero CEP suggests that they originate from the same physical effects. Summarizing this qualitative analysis, we conclude that:

- the zero-order terms of the asymptotic series of Eqs. (14) through (22) are characteristic to the monochromatic approximation of the original Keldysh model [54] that assumes constant oscillation amplitude within each single oscillation cycle;

- the terms of the order of $1/\alpha$ of the asymptotic series are attributed to the violation of the homogeneous sub-cycle distribution of the electron (and hole) oscillation amplitude within each oscillation cycle;

- the terms of the order of $1/\alpha^2$ correspond to the delay effects associated with the rate at which the sub-cycle amplitude-distribution is violated.

This interpretation is supported by simulations of separated contributions of those terms into the overall modification of the energy bands (Fig. 5). In particular, if the pulse envelope is symmetric with respect to the pulse peak, the inhomogeneous sub-cycle distribution of the oscillation amplitude must produce zero mutual p-shift of the energy bands at any CEP at the pulse peak if the delay effects are neglected and corresponding $1/\alpha^2$ and $1/\alpha^3$ terms are omitted (Fig. 5(b)). It results from the fact that the oscillation amplitude is the same for both halves of the cycle centered at the pulse peak (Fig. 6). This is perfectly confirmed by simulations of the mutual band p-shift with the series containing only the zero-order and the $1/\alpha$ terms (Fig. 5(b)). The terms of the order of $1/\alpha^2$ attributed to the delay effects produce a non-zero band p-shift at the pulse peak (Fig. 5(b)). The delay terms also disturb the symmetric positions of the maxima and minima of the p-shifts with respect to the pulse peak in the time domain (see Eqs. (25) through (28)).

Certain physical meaning could also be assigned to the terms of the order of $1/\alpha^3$, but they are of minor value and are retained mainly for improvement of the accuracy at reduced pulse width (Fig. 5).

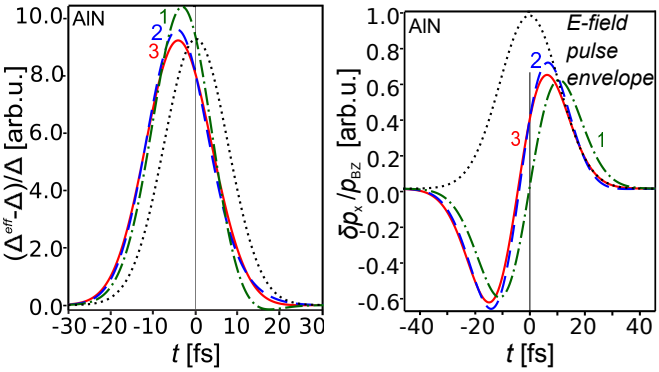

FIG. 5. (a) Normalized difference between the effective direct band gap and the original band gap of AlN evaluated with the different terms of Eq. (21): black dashed – only zero-order terms (i.e., the monochromatic model of Eq. (23)); green dash-dotted curve 1 – zero- and first-order terms; blue dashed curve 2 – zero-, first-, and second-order terms; red solid curve 3 – the terms of all orders from zero to the third inclusive. Laser-pulse parameters are the same as in Fig. 4(b), peak intensity is 30 TW/cm^2. (b) Normalized mutual band p-shifts along the momentum direction collinear with laser-pulse electric field evaluated with different terms of Eq. (19): green dash-dotted curve 1 – first-order terms; blue dashed curve 2 – first- and second-order terms; red solid curve 3 – all the terms from zero to the third order inclusive. Laser parameters are the same as in Fig. 3(b). The vertical lines depict instant of the pulse peak.

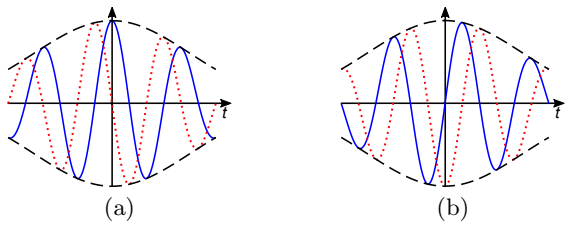

FIG. 6. (a) A sketch of the instant variations of the electric field (blue solid) and electron momentum (red dot) in the time domain for the zero (a) and $\pi/2$ (b) CEP. Black dashed line depicts the pulse envelope. The time variations of the electron momentum and electric field are normalized so as to follow the same slow envelope.

IV.2. Parametric scaling of the band modifications

Scaling with six laser and material parameters is delivered by the analytical relations of Section III.1 (see Table II). The band-structure modifications under consideration are enhanced by reduction of pulse width and reduction of the Keldysh adiabatic parameter. The latter can be reduced, for example, by increasing the peak intensity of a laser pulse. Therefore, at a fixed pulse width, the higher peak laser intensity, the stronger the pulse-driven features of the transient bands discussed above. Also, the band shifts are more pronounced in crystals with smaller band gaps due to the reduction of the Keldysh parameter (Figs. 2, 3, and 4). Finally, the

TABLE II. Scaling of the key parameters of the non-monochromatic modifications of the band structure with carrier wavelength λ, peak pulse intensity I_0, initial band gap Δ, reduced effective electron-hole mass m_0, and pulse width τ_p.

Band-structure parameter	Equation(s)	Scaling with pulse and adiabatic parameters	Scaling with laser and material parameters
Maximum non-monochromatic correction to the direct and indirect effective band gap (e.g., Eq. (20) minus Eq. (23))	(20), (21), (23)	$1/(\alpha\gamma_0^2)$	$\lambda^3 I_0/(m_0\Delta\tau_p)$
Absolute value of the mutual p-shift of the energy bands at the CEP $\phi_0 \neq \pi/2 \pm N\pi$, $N=0,1,2,\ldots$	(19)	$1/(\alpha\gamma_0)$	$\lambda^2 I_0^{1/2}/(m_0^{1/2}\Delta^{1/2}\tau_p)$
Absolute value of the mutual p-shift of the energy bands at the CEP $\phi_0 = \pi/2 \pm N\pi$, $N=0,1,2,\ldots$	(19)	$1/(\alpha^2\gamma_0)$	$\lambda^3 I_0^{1/2}/(m_0^{1/2}\Delta^{1/2}\tau_p^2)$

specific pulse-driven contributions to the band modification become more pronounced with the increase of laser wavelength.

Influence of another key material parameter – effective electron/hole mass – is less trivial. First, we note that the effective masses are not modified under the considered approximations, and the energy bands are shifted without deformation during the laser-driven modifications. This conclusion is evident from the Eqs. (14) and (15). Second, reduction of the effective masses favors reduction of the adiabatic parameter and, therefore, low-effective-mass crystals are more favorable for observation of the reported effects. Third, if the valence-band effective mass significantly exceeds the conduction-band mass (that is the case for typical dielectric crystals), the difference between the effective direct and indirect band gaps reduces according to Eqs. (20) and (21). The physical reason for this conclusion is quite transparent: $m_{VB} >> m_{CB}$ means the valence band is almost flat, and the p-shift of the effective conduction band away from its initial position does not remarkably contribute to the difference between the direct and indirect effective band gaps. If the effective masses do not differ very much, the effective direct band gap becomes larger than the indirect band gap, and the difference between them is of the order of $1/(\alpha^2\gamma_0^2)$. Therefore, the indirect-gap structure of the transient energy bands is expected to produce a stronger effect on the laser-driven processes in typical semiconductors.

Finally, we note a strong influence of CEP on the transient bands. It can be interpreted in terms of a specific dephasing between the driving electric field and the laser-driven electron/hole oscillations. For example, if the delay effects are neglected, the oscillation amplitude is symmetrically distributed between the two halves of the oscillation cycle centered at the pulse peak at any CEP (Fig. 6). This fact suggests zero p-shift of the energy bands with respect to each other at the pulse peak. Therefore, the delay effects are the only to make a non-zero contribution to the band p-shift at the pulse peak. That contribution is of the order of $1/(\alpha^2\gamma_0)$ at any CEP since the rate of the time variations of the pulse envelope $f'(t)$ is zero. However, with the accuracy of the $1/\alpha$ terms, the zero CEP produces zero instant electron departure from an initial state at the pulse peak (Fig. 6(a)), and the delay effects make a minor contribution to the zero value of the p-shift. In opposite, the $\pi/2$ CEP delivers the maximum instant electron/hole departure from the initial state at the pulse peak (Fig. 6(b)), and the delay effects make the only contribution to the maximum p-shift of the energy bands at the pulse peak, but that contribution is of the order of $1/(\alpha^2\gamma_0)$. That is, the delay effects determine minimum p-shift of the bands at CEP=0 and maximum p-shift at CEP=$\pi/2$ at the laser-pulse peak. This dephasing explains the suppression of the band p-shift at CEP close to $(\pi/2 \pm N\pi)$.

IV.3. Competing mechanisms of band-structure modification

The reported band-structure modifications consider the only mechanism associated with the laser-driven electron/hole oscillations. In semiconductor crystals, there may be other mechanisms contributing to laser-induced modifications of band gap and energy bands. For example, the high-frequency Franz-Keldysh effect [78, 79]; laser-enhanced coupling of valence and conduction bands [80–82]; band-gap shrinkage due to increase of conduction-band electron density [82, 83]; and band filling [82–85] (also referred to as Burstein-Moss effect [83]) are among the mechanisms competing with the laser-driven oscillations. Except for the Burstein-Moss effect, those mechanisms reduce the initial band gap, i.e., compete with the band-gap increase by the ponderomotive energy of the electron and hole oscillations. However, the Franz-Keldysh effect and the band coupling are significant for narrow-gap semiconductors with initial band gap about 1 eV or smaller [78–82]. A large band gap between the lowest conduction band and the highest valence band of the wide-band-gap crystals significantly suppresses those mechanisms. Moreover, the band-gap variations by the Franz-Keldysh effect scale as $E_0^{3/2}$ with electric-field amplitude E_0 of the high-intensity laser-pulse [78, 79] while the contribution of the laser-driven electron/hole oscillations results in E_0^2 scaling. Therefore, it is reasonable to expect that the laser-driven oscillations dominate over the Franz-Keldysh effect in the wide-band-gap crystals at high intensity.

The band-gap variation due to the shrinkage effect can

be evaluated using the equations of Refs. [82, 83, 85]. Those estimations deliver the band gap reduction by a few tenths of eV at the highest conduction-band electron density 10^{19}–10^{20} 1/cm^3 recently reported at sub-damage-threshold irradiance [8, 16, 18, 23]). Those values are substantially smaller than the increase of the effective band gap by several eV produced by the laser-driven oscillations. Therefore, the band-gap shrinkage can be neglected in the first approximation. Generation of the conduction-band electrons by the inter-band excitation can also contribute to the band-gap modification due to the band filling effect [82, 83, 85]. In general, that modification can be as large as an energy of a few laser photons since the absence of vacant states at the bottom of the conduction band favors absorption of one extra photon to promote the newly arriving electrons to vacant states of the band. However, the influence of the band filling effect is very unlikely in the case under consideration since an ultrashort laser pulse generates electron population in a broad range of states first on the one side of the conduction band (at the leading edge of the pulse) and then on the opposite side of the band (at the tail edge of the pulse) due to the mutual band p-shift.

Therefore, the laser-driven electron/hole oscillations are expected to dominantly contribute to the band-structure modifications of the wide-band-gap crystals during the immediate action of an ultrashort high-intensity laser pulse.

IV.4. Slowly varying electron current

Another remarkable effect produced by the non-monochromatic laser-driven electron/hole oscillations is the electric current driven by the pulse envelope. Its generation becomes evident from a relation for the electron momentum of Eq. (10) when it is averaged over a single oscillation cycle:

$$\langle p_{xe}\rangle(s) = p_{x0} - \sqrt{m_{CB}\Delta}\left[\frac{f'(s)}{\alpha\gamma_{CB}}\cos(\phi_0) - \frac{f''(s)}{\alpha^2\gamma_{CB}}\Psi_{x1} - \frac{f'''(s)}{\alpha^3\gamma_{CB}}\Psi_{x2}\right]. \quad (36)$$

A similar relation is true for the oscillating holes. Eq. (36) contains the non-zero field-dependent component that corresponds to photocurrent in the direction parallel to the laser-pulse electric field. Comparing Eq. (36) with Eq. (19), one notices that the time variations and the parametric scaling of the current are similar to the variations of the mutual band p-shift. This photo-current results from a dominant promotion of the oscillating electrons (holes) in a direction parallel to the electric field of the linearly-polarized laser pulse. In turn, that promotion of the free carriers in the real physical space arises from the violation of the sub-cycle symmetry of the oscillation amplitude discussed in Section II.2. To estimate the charge it produces, we evaluate the peak value of electron current density j_{eMAX} via the peak value p_{eM} of the field-induced part of Eq. (36), maximum free-carrier density n_{eMAX}, and effective conduction-band mass as follows [46]:

$$j_{eMAX} = \frac{q\cdot n_{eMAX}\cdot p_{eM}}{m_{CB}}. \quad (37)$$

We further assume the current is generated in a focal volume characterized by an effective radius R of the order of 10^{-6}–10^{-5} m. Simulations of the laser-induced free-carrier dynamics [8, 12] show that free-electron density reaches significant values only after the peak of an ultrashort laser pulse, i.e., over the tail part of the pulse. Therefore, the total charge produced by the current is the most effectively accumulated over the time interval of the order of τ_p. For the laser-pulse parameters from the caption of Fig. 3 and the material parameters of Table I, the photo-current density is estimated as 10^{11}–10^{13} A/cm^2 if maximum laser-induced free-carrier density is 10^{20}–10^{22} 1/cm^3 respectively. Correspondingly, the photo-charge delivered by the photocurrent varies from 1 to 100 nC for that range of free-electron density.

It is remarkable that the mechanism of this ultrafast photo-current generation differs from that of recently reported photocurrent effects driven by an instant electric field of two-cycle laser pulses in dielectrics [36, 37]. Also, the photocurrent predicted by Eq. (36) is a few orders of magnitude larger than that reported in Refs. [36] and [37] and it can produce a significant contribution to the transient optical response. Detailed analysis of those effects substantially goes beyond the scope of this paper.

IV.5. Indirect-gap crystals

The modification of the energy bands considered above assumes direct-gap structure prior to the laser action. It is shown that the direct-gap band structure is not conserved during the laser action on the crystal, and the crystal responses as an indirect-gap one. For typical indirect-gap crystals, the bottom of the conduction band is displaced by p_S away from the center of the Brillouin zone alone one of the crystal axes prior to the laser action [46, 64]. That feature of the indirect-gap bands substantially influences the laser-driven band-structure modification only if the electric field of a laser pulse is directed along that crystal axis (it is considered as axis x to be specific). A majority of the relations presented above for the direct-gap crystals is still valid in that case if the momentum component px and its normalized values (i.e., x_{CB} for the conduction band and x_{VB} for the valence band) are replaced with $p_x - p_S$, $x_{CB} - x_S$, and $x_{VB} - x_S$ correspondingly. The only relation that receives a significant modification beyond that substitution is the Eq. (21) for the effective direct band gap. However, the approximation of the parabolic bands is not sufficient to properly evaluate the effective direct band gap of the indirect-gap crystals since the initial band displacement p_S is usually so large [46] that non-parabolic features of the energy bands cannot be neglected. Ultrafast modi-

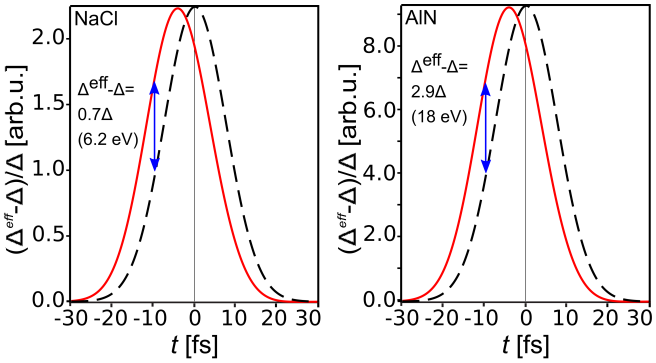

(a) (b)

FIG. 7. Illustration of expected influence of the laser-induced p-shift of the energy bands on the rate of the photoionization. The data are the same as in Fig. 4 (a).

fication of non-parabolic bands requires a separate consideration to be reported in the nearest future.

IV.6. Potential influence of the non-monochromatic effects on the photoionization

The specific variations of the band structure by the laser-driven electron oscillations are favorable for some qualitative analysis of the photoionization and nonlinear absorption. The analysis is based on the fundamental exponential dependence of the inter-band transition rate on effective band gap [46, 54]. First, the time-domain dynamics of the effective band gaps suggest suppression of the photoionization at the leading edge of an ultrashort laser pulse compared to the predictions of the monochromatic Keldysh model [54]. This suppression results from a significant enhancement of the effective direct band gap of the pulse-driven model compared to the monochromatic approach (Fig. 7). The difference between those models can be as large as few eV and is more pronounced in wide-band-gap semiconductors (Fig. 7). Therefore, the pulse-driven model predicts absorption of a few more photons at the leading edge of the pulse compared to the estimations by the monochromatic Keldysh model. The photoionization suppression due to the increase of the effective band gap is enhanced by the reduced laser intensity at the leading tail of the pulse (Fig. 7). The action of those two processes favors formation of an abrupt front (within very few cycles) of the photoionization. The situation is reversed at the tail part of the laser pulse where the pulse-driven model predicts lower effective band gap than that of the monochromatic approximation. This specific feature of the pulse-driven modification of the band structure should lead to substantial enhancement of the photoionization and the nonlinear absorption at the tail part of the pulse. This violation of the temporal symmetry of the nonlinear absorption with respect to the pulse peak may result in specific time dynamics of the nonlinear optical response as well as energy absorption and transfer.

V. CONCLUSIONS

In conclusion, we have reported the transient bands formed by the ponderomotive energy of the ultrashort pulses of laser-driven electron/hole oscillations in a wide-band-gap crystal. The monochromatic and quasi-monochromatic approximations assume the homogeneous distribution of the oscillation amplitude within every single cycle. Departure from the monochromatic approximation is done by taking into account the fundamental fact that the amplitude of the second half of any oscillation cycle is never the same as the amplitude of the first half of the cycle. This basic property of the ultrashort oscillation pulses results in the formation of the transient indirect-gap band structure due to the p-shifting of the original bands in the direction parallel to the electric field of the laser pulse. The transient bands are characterized by the effective direct and indirect band gaps. Another specific feature of the ultrashort-pulse-driven modification of the energy bands is the shift of the maximum of the time-dependent direct effective band gap away from the peak of a laser pulse in the time domain. Due to that shift, the effective pulse-driven band gap exceeds that of the monochromatic approximation at the leading part of a laser pulse. At the tail part of the pulse, the situation is reversed, i.e., the ultrashort-pulse model predicts a smaller effective band gap compared to that of the monochromatic approach. This feature suggests a significant suppression of the laser-induced photoionization and associated nonlinear absorption at the leading edge of the ultrashort laser pulse and possible formation of an abrupt ionization front. Finally, the reported above model predicts generation of a slowly-varying photo-current of free carriers driven by the pulse envelope. It can make a specific contribution to the ultrafast optical response of the crystals. All those results are obtained under the assumption that the laser-driven oscillations dominantly contribute to the band-structure distortions in the crystals.

The reported model suggests that the Keldysh formula for the photoionization rate of crystals [54] can be a reasonable approximation for a domain of laser and material parameters that provide large value of the products $(\alpha\gamma_0^2)$ and $(\alpha\gamma_0)$. For few-cycle and high-intensity laser pulses, the Keldysh formula cannot deliver any reasonable estimation of the photoionization rate because it incorporates incorrect estimation of the effective band gap.

The reported model can serve as an improved basis for theoretical evaluation of the time-dependent nonlinear absorption and transient optical response of the wide-band-gap crystals during an immediate action of the high-intensity ultrashort laser pulses on the crystals.

VI. ACKNOWLEDGEMENTS

Fruitful discussions and comments of Dr. Alexander Rubenchik (Lawrence Livermore National Laboratory, USA) and Dr. Vladislav Yakovlev (Max Plank Insti-

tute of Quantum Optics, Germany) are greatly acknowledged. This material is based upon work supported by the Air Force Office of Scientific Research under award number FA9550-15-1-0254.

[1] P. Balling and J. Schou, Rep. Prog. Phys. **76**, 036502 (2013).
[2] B. Rethfeld, D. S. Ivanov, M. E. Garcia, and S. I. Anisimov, J. Phys. D: Appl. Phys. **50**, 193001 (2017).
[3] O. Utéza, N. Sanner, B. Chimier, A. Brocas, N. Varkentina, M. Sentis, P. Lassonde, F. Légaré, and J. C. Kieffer, Appl. Phys. A **105**, 131 (2011).
[4] M. Lebugle, N. Sanner, O. Utéza, and M. Sentis, Appl. Phys. A **114**, 129 (2014).
[5] A. Mouskeftaras, S. Guizard, N. Fedorov, and S. Klimentov, Appl. Phys. A **110**, 709 (2013).
[6] C. Pasquier, M. Sentis, O. Utza, and N. Sanner, Appl. Phys. Lett. **109**, 051102 (2016).
[7] B. Chimier, O. Utéza, N. Sanner, M. Sentis, T. Itina, P. Lassonde, F. Légaré, F. Vidal, and J. C. Kieffer, Phys. Rev. B **84**, 094104 (2011).
[8] S. Mao, F. Quéré, S. Guizard, X. Mao, R. Russo, G. Petite, and P. Martin, Appl. Phys. A **79**, 1695 (2004).
[9] M. Lenzner, J. Krüger, S. Sartania, Z. Cheng, C. Spielmann, G. Mourou, W. Kautek, and F. Krausz, Phys. Rev. Lett. **80**, 4076 (1998).
[10] D. Grojo, S. Leyder, P. Delaporte, W. Marine, M. Sentis, and O. Utéza, Phys. Rev. B **88**, 195135 (2013).
[11] Q. Meng, B. Zhang, S. Zhong, and L. Zhu, Appl. Phys. A **122**, 582 (2016).
[12] L. A. Emmert and W. Rudolph, "Femtosecond laser-induced damage in dielectric materials," in *Laser-Induced Damage in Optical Materials*, edited by D. Ristau (CRC Press, Taylor and Francis Group, Boca Raton, 2015) Chap. 5, p. 127.
[13] K. R. P. Kafka, N. Talisa, G. Tempea, D. R. Austin, C. Neacsu, and E. A. Chowdhury, Opt. Express **24**, 28858 (2016).
[14] N. Sanner, O. Utéza, B. Chimier, M. Sentis, P. Lassonde, F. Légaré, and J. C. Kieffer, Appl. Phys. Lett. **96**, 071111 (2010).
[15] J. Cheng, M. Chen, K. Kafka, D. Austin, J. Wang, Y. Xiao, and E. Chowdhury, AIP Adv. **6**, 035221 (2016).
[16] V. V. Temnov, K. Sokolowski-Tinten, P. Zhou, A. El-Khamhawy, and D. von der Linde, Phys. Rev. Lett. **97**, 237403 (2006).
[17] H. Dachraoui, C. Oberer, and U. Heinzmann, Opt. Express **19**, 2797 (2011).
[18] D. G. Papazoglou, D. Abdollahpour, and S. Tzortzakis, Appl. Phys. A **114**, 161 (2014).
[19] S. Juodkazis, V. Mizeikis, S. Matsuo, K. Ueno, and H. Misawa, Bull. Chem. Soc. Jpn. **81**, 411 (2008).
[20] A. Rudenko, J.-P. Colombier, and T. E. Itina, Phys. Rev. B **93**, 075427 (2016).
[21] J. R. Gulley, S. W. Winkler, W. M. Dennis, C. M. Liebig, and R. Stoian, Phys. Rev. A **85**, 013808 (2012).
[22] J. R. Gulley and T. E. Lanier, Phys. Rev. B **90**, 155119 (2014).
[23] L. Sudrie, A. Couairon, M. Franco, B. Lamouroux, B. Prade, S. Tzortzakis, and A. Mysyrowicz, Phys. Rev. Lett. **89**, 186601 (2002).
[24] S. Skupin and L. Berg, Physica D **220**, 14 (2006).
[25] National Academies of Sciences, Engineering, and Medicine, *Opportunities in Intense Ultrafast Lasers: Reaching for the Brightest Light* (The National Academies Press, Washington, DC, 2018).
[26] S. Ghimire, A. D. DiChiara, E. Sistrunk, P. Agostini, L. F. DiMauro, and D. A. Reis, Nat. Phys. **7**, 138 (2011).
[27] S. Ghimire, A. D. DiChiara, E. Sistrunk, G. Ndabashimiye, U. B. Szafruga, A. Mohammad, P. Agostini, L. F. DiMauro, and D. A. Reis, Phys. Rev. A **85**, 043836 (2012).
[28] S. Ghimire, G. Ndabashimiye, A. D. DiChiara, E. Sistrunk, M. I. Stockman, P. Agostini, L. F. DiMauro, and D. A. Reis, J. Phys. B: At., Mol. Opt. Phys. **47**, 204030 (2014).
[29] P. Földi, M. G. Benedict, and V. S. Yakovlev, New J. Phys. **15**, 063019 (2013).
[30] O. Schubert, M. Hohenleutner, F. Langer, B. Urbanek, C. Lange, U. Huttner, D. Golde, T. Meier, M. Kira, S. W. Koch, and R. Huber, Nat. Photonics **8**, 119 (2014).
[31] S. Y. Kruchinin, M. Korbman, and V. S. Yakovlev, Phys. Rev. B **87**, 115201 (2013).
[32] C. R. McDonald, G. Vampa, P. B. Corkum, and T. Brabec, Phys. Rev. A **92**, 033845 (2015).
[33] G. Vampa, C. R. McDonald, G. Orlando, D. D. Klug, P. B. Corkum, and T. Brabec, Phys. Rev. Lett. **113**, 073901 (2014).
[34] G. Vampa, C. R. McDonald, G. Orlando, P. B. Corkum, and T. Brabec, Phys. Rev. B **91**, 064302 (2015).
[35] M. S. Wismer, S. Y. Kruchinin, M. Ciappina, M. I. Stockman, and V. S. Yakovlev, Phys. Rev. Lett. **116**, 197401 (2016).
[36] M. Schultze, E. M. Bothschafter, A. Sommer, and S. H. et. al., Nature **493**, 75 (2013).
[37] A. Schiffrin, T. Paasch-Colberg, N. Karpowicz, V. Apalkov, D. Gerster, S. Mühlbrandt, M. Korbman, J. Reichert, M. Schultze, S. Holzner, J. V. Barth, R. Kienberger, R. Ernstorfer, V. S. Yakovlev, M. I. Stockman, and F. Krausz, Nature **493**, 70 (2013).
[38] M. Korbman, S. Y. Kruchinin, and V. S. Yakovlev, New J. Phys. **15**, 013006 (2013).
[39] M. Wu, S. Ghimire, D. A. Reis, K. J. Schafer, and M. B. Gaarde, Phys. Rev. A **91**, 043839 (2015).
[40] T. Higuchi, M. I. Stockman, and P. Hommelhoff, Phys. Rev. Lett. **113**, 213901 (2014).
[41] P. G. Hawkins, M. Y. Ivanov, and V. S. Yakovlev, Phys. Rev. A **91**, 013405 (2015).
[42] O. Kwon, T. Paasch-Colberg, V. Apalkov, B.-K. Kim, J.-J. Kim, M. I. Stockman, and D. Kim, Sci. Rep. **6**, 21272 (2016).
[43] C. R. McDonald, G. Vampa, P. B. Corkum, and T. Brabec, Phys. Rev. Lett. **118**, 173601 (2017).
[44] P. A. Zhokhov and A. M. Zheltikov, Phys. Rev. Lett. **113**, 133903 (2014).
[45] S. Lagomarsino, S. Sciortino, B. Obreshkov, T. Apostolova, C. Corsi, M. Bellini, E. Berdermann, and C. J. Schmidt, Phys. Rev. B **93**, 085128 (2016).
[46] N. W. Ashkroft and N. D. Mermin, *Solid State Physics* (Saunders College Publishing, New York, 1976).
[47] L. D. Landau and E. M. Lifshitz, *Quantum Mechanics* (Pergamon Press, New York, 1958).

[48] E. Runge and E. K. U. Gross, Phys. Rev. Lett. **52**, 997 (1984).

[49] E. K. U. Gross, J. F. Dobson, and M. Petersilka, "Density functional theory of time-dependent phenomena," in *Density Functional Theory II: Relativistic and Time Dependent Extensions*, edited by R. F. Nalewajski (Springer Berlin Heidelberg, Berlin, Heidelberg, 1996) pp. 81–172.

[50] T. Otobe, K. Yabana, and J.-I. Iwata, Phys. Rev. A **69**, 053404 (2004).

[51] H. Akagi, T. Otobe, A. Staudte, A. Shiner, F. Turner, R. Dörner, D. M. Villeneuve, and P. B. Corkum, Science **325**, 1364 (2009).

[52] T. Otobe, M. Yamagiwa, J.-I. Iwata, K. Yabana, T. Nakatsukasa, and G. F. Bertsch, Phys. Rev. B **77**, 165104 (2008).

[53] T. Otobe, K. Yabana, and J.-I. Iwata, J. Phys.: Condens. Matter **21**, 064224 (2009).

[54] L. V. Keldysh, Sov. Phys. JETP **20**, 1307 (1965).

[55] M. Y. Ivanov, M. Spanner, and O. Smirnova, J. Mod. Opt. **52**, 165 (2005).

[56] Y. A. Bychkov and A. Dykhne, Sov. Phys. JETP **31**, 928 (1970).

[57] V. A. Kovabskii and E. Y. Perlin, Physica Status Solidi B **45**, 47 (1971).

[58] H. D. Jones and H. R. Reiss, Phys. Rev. B **16**, 2466 (1977).

[59] V. E. Gruzdev, Phys. Rev. B **75**, 205106 (2007).

[60] A. Bourgeade and G. Duchateau, Phys. Rev. E **85**, 056403 (2012).

[61] C. Mezel, G. Duchateau, G. Geneste, and B. Siberchicot, J. Phys.: Condens. Matter **25**, 235501 (2013).

[62] J. R. Gulley, Opt. Eng. **51**, 121805 (2012).

[63] V. E. Gruzdev, J. Opt. Technol. **71**, 504 (2004).

[64] F. Bassani and G. P. Parravicini, *Electronic States and Optical Transitions in Solids* (Pergamon Press, New York, 1975).

[65] D. von der Linde and K. Sokolowski-Tinten, Appl. Surf. Sci. **154-155**, 1 (2000).

[66] L. V. Keldysh, Sov. Phys. JETP **6**, 763 (1958).

[67] L. V. Keldysh, Sov. Phys. JETP **7**, 788 (1958).

[68] J. B. Krieger and G. J. Iafrate, Phys. Rev. B **33**, 5494 (1986).

[69] H. Kurz, H. G. Roskos, T. Dekorsy, and K. Köhler, Philosophical Transactions of the Royal Society of London A: Mathematical, Physical and Engineering Sciences **354**, 2295 (1996).

[70] T. Hartmann, F. Keck, H. J. Korsch, and S. Mossmann, New J. Phys. **6**, 2 (2004).

[71] P. C. Becker, H. L. Fragnito, C. H. BritoCruz, R. L. Fork, J. E. Cunningham, J. E. Henry, and C. V. Shank, Phys. Rev. Lett. **61**, 1647 (1988).

[72] D. B. Sirdeshmukh, L. Sirdeshmukh, and K. G. Subhadra, *Alkali Halides: A Handbook of Physical Properties* (Springer-Verlag, Berlin, 2001).

[73] H. Morkoc, *General Properties of Nitrides, in Handbook of Nitride Semiconductors and Devices: Materials Properties, Physics and Growth*, Vol. 1 (Wiley-VCH Verlag GmbH and Co. KGaA, Weinheim, Germany, 2008).

[74] *See Supplemental Materials 1 and 2 at [URL will be inserted by publisher] for animation of the real-time variations of the valence and conduction bands of NaCl and AlN*.

[75] *See Supplemental Materials 3 and 4 at [URL will be inserted by publisher] for animations of time variations of wavelength scaling of the deviations between initial band gap, and effective direct and effective indirect band gaps of NaCl and AlN normalized to the initial band gap*.

[76] O. N. Sergaeva and V. E. Gruzdev, in *Conference on Lasers and Electro-Optics* (Optical Society of America, 2017) p. JTh2A.28.

[77] O. Sergaeva and V. Gruzdev, in *Proc. URSI-GASS, Montreal, Canada, 19-26 August 2017* (2017).

[78] Y. Yacoby, Phys. Rev. **169**, 610 (1968).

[79] T. Otobe, Y. Shinohara, S. A. Sato, and K. Yabana, Phys. Rev. B **93**, 045124 (2016).

[80] Y. Mizumoto and Y. Kayanuma, Phys. Rev. B **72**, 115203 (2005).

[81] Y. Mizumoto, Y. Kayanuma, A. Srivastava, J. Kono, and A. H. Chin, Phys. Rev. B **74**, 045216 (2006).

[82] S. S. Prabhu and A. S. Vengurlekar, J. Appl. Phys. **95**, 7803 (2004).

[83] B. R. Bennett, R. A. Soref, and J. A. D. Alamo, IEEE J. Quantum. Electron. **26**, 113 (1990).

[84] P. A. Wolff, Phys. Rev. **126**, 405 (1962).

[85] Y. H. Lee, A. Chavez-Pirson, S. W. Koch, H. M. Gibbs, S. H. Park, J. Morhange, A. Jeffery, N. Peyghambarian, L. Banyai, A. C. Gossard, and W. Wiegmann, Phys. Rev. Lett. **57**, 2446 (1986).